JOURNAL OF MATERIALS SCIENCE 26 (1991) 2823–2832

The stress-whitened damage zone of PVC blends

A. TSE, E. SHIN, A. HILTNER, E. BAER
Department of Macromolecular Science and Center for Applied Polymer Research Case Western Reserve University Cleveland, OH 44106, USA

R. LAAKSO
Louisiana Division, The Dow Chemical Company, Plaquemine, LA 70765, USA

The stress-whitened damage zone that formed ahead of a semicircular notch during slow tensile loading has been measured from optical micrographs of translucent blends of poly(vinyl chloride) (PVC) with experimental chlorinated polyethylene (CPE) resins. When the zone was small, the plane strain condition applied and from the elastic stress distribution a constant mean stress condition was found at the boundary of the crescent-shaped zone. The critical mean stress did not depend on the chlorine content or the chlorine distribution of the experimental CPE resin used in the blend. While the critical mean stress decreased as the amount of CPE in the blend was increased, the critical volume strain, calculated from the bulk modulus, was independent of composition and was thought to be the controlling parameter for stress-whitening. When the zone was larger, the shape was qualitatively described by concepts of stress redistribution in the presence of a plastic zone ahead of the notch. Macroscopic flow and necking were only detected near the maximum in the stress–displacement curve.

1. Introduction

Substantial enhancement of toughness can be achieved by dispersing rubber particles within a polymer matrix. Cavitation of the rubber particles and plastic hole growth to create a damage zone in the region of the crack tip is a general mechanism of toughening in these materials. Toughening of poly(vinyl chloride) (PVC) by chlorinated polyethylene (CPE) is one example where toughening is achieved by this voiding mechanism [1, 2].

It has been recognized that dilation, except for crazing, can be very small in uniaxial tests where essentially all the deformation occurs by shear [3]. Significant voiding occurs only in the neck region where a triaxial state of stress develops. By contrast, substantial void nucleation and growth occurs in the plastic zone around a crack. Consequently, uniaxial tests can be seriously misleading in predicting failure at a crack tip where the stress state is triaxial. The importance of the mean stress is extensively illustrated by the failure of ductile metals which depends on nucleation and growth of voids at a second phase. It follows that the role of dilation in toughening of rubber-toughened materials can only be directly measured in tests utilizing stress states with significant degree of triaxiality.

The sharp notch geometry is frequently used for observations in triaxial tension because the stress state approximates that at the tip of the propagating crack. Other geometries have also been used. The circular or semicircular notch is particularly attractive when the objective is to examine the damage zone while minimizing the tendency for crack growth. For example, examination of the shear yielding modes at a semicircular notch has clarified the effect of sheet thickness on the ductility of polycarbonate [4].

Most toughened plastics are not readily amenable to studies of cavitation in thick notched sheets. The optimum rubber particle size for toughening also produces the maximum light scattering and optical opacity so that stress-whitening is not readily distinguishable by optical techniques. By matching refractive indices, impact modifiers have been developed that produce transparent or translucent blends. In a recent study of the optical properties of PVC toughened with CPE, several experimental CPE resins were identified that produced translucent blends by refractive index matching [5]. These are now used to measure the stress-whitened zone in toughened PVC under triaxial tension.

2. Experimental procedure

Blends of a low molecular weight poly(vinyl chloride) (Georgia Gulf 2066, $K = 55$) with 5, 10, 15 or 20 p.p.h. of an experimental chlorinated polyethylene (CPE) resin were prepared as described previously [5]. The blends also contained 2.5 p.p.h. of a heat stabilizer (Mark 1900, Argus Chemical), 1.5 p.p.h. of a processing aid (Paraloid K-175, Rohm and Haas), 1.5 p.p.h. of an internal lubricant (Loxiol HOB 7111, Henkel Corporation) and 0.3 p.p.h. of a u.v. stabilizer

0022–2461/91 $03.00 + .12

(Tinuvin 328, Ciba-Geigy). The blends were supplied by The Dow Chemical Company, Louisiana Division, Plaquemine, LA, in the form of 1.5 mm thick roll-milled blankets. The components had been dry blended, then roll-milled at 175 °C for 5 min after fusion. Specimens of the desired thickness were moulded in a preheated press at 175 °C at 2000 psi for 5 min, cooled under pressure and annealed at 80 °C for 4 h. Experimental resin 5896 produced blends with the highest optical transparency and these were chosen for the most detailed studies.

Tensile tests were carried out on notched rectangular bars 152 × 20 mm^2 of two thicknesses, 1.6 and 3.6 mm. The 1 mm radius semicircular notch was machined midway along one edge. Tests were performed on an Instron machine at ambient temperature with a crosshead speed of 0.1 mm min^{-1}, the separation of the grips when the specimen was mounted was 100 mm. The damage zone at the notch was photographed during loading with a travelling optical microscope in the transmission mode at a magnification of 28 × . In some cases, specimens were loaded to a specific position on the stress–displacement curve, then removed from the Instron for further examination. These specimens were either polished with silicon carbide paper of successively finer grades and then with suspensions of aluminium oxide powder down to 0.1 μm, or were cut into approximately 0.4 mm thick sections with a low speed, water cooled Isomet saw. The sections were viewed with an Olympus Model BH2 optical microscope in the transmission mode.

The Young's modulus and yield stress were obtained from tensile tests at ambient temperature of 3.6 mm thick specimens prepared according to the ASTM D638 Type I geometry with an extensometer to measure strain. The crosshead speed was 10 mm min^{-1} which produced a strain rate of 20 % min^{-1}. This strain rate was estimated to be the equivalent of the effective strain rate at the notch root under the conditions that were used to test the notched specimens [6].

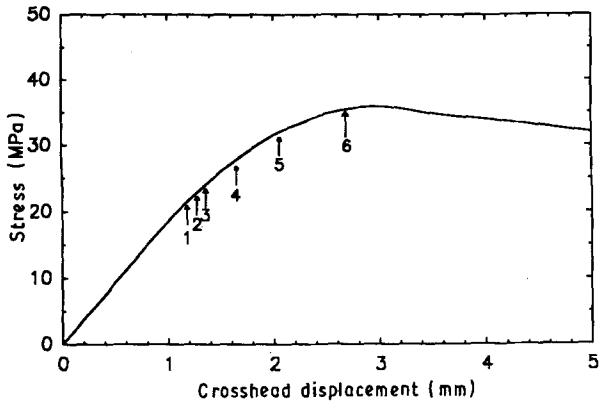

Figure 1 Stress–displacement curve of 3.6 mm thick PVC with 15 p.p.h. experimental resin 5896.

3. Results and discussion

3.1. Damage zone

The stress–displacement curve of a PVC blend with 15 parts of the experimental resin 5896 is shown in Fig. 1. The curve consisted of a linear region up to about 18 MPa and 1.0 mm crosshead displacement, then a non-linear region with a stress maximum at 36.5 MPa. The 3.6 mm thick specimen with a semicircular notch was photographed during deformation, and the arrows indicate the positions at which the micrographs shown in the following sequence were taken. The first visible damage was stress-whitening due to a cavitation mechanism [1] that occurred near the linear limit of the stress–displacement curve. The clearest image of the damage region was obtained when it was photographed with the focus at the centre of the specimen. At position 1 in Fig. 1, a small curved zone of stress-whitening was visible ahead of the notch (21.6 MPa, Fig. 2a). The zone increased in size successively at position 2 (22.7 MPa, Fig. 2b) and at position 3 (23.8 MPa, Fig. 2c), but maintained the same cres-

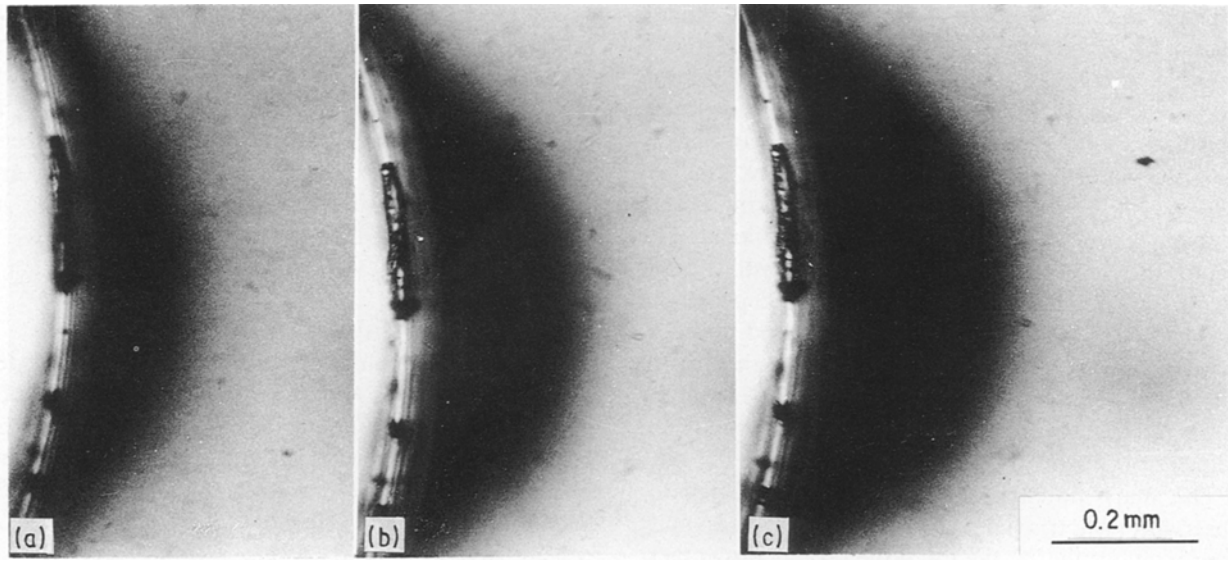

Figure 2 Optical micrographs of stress-whitened zone of 3.6 mm thick PVC with 15 p.p.h. experimental resin 5896. (a) Position 1, 21.6 MPa, (b) position 2, 22.7 MPa, and (c) position 3, 23.8 MPa.

cent shape. At higher stresses the shape changed and the damage zone became elongated ahead of the notch.

3.2. Elastic stress distribution at a semicircular notch

The condition for stress-whitening was determined from the stress state at the boundary between the damage zone and the non-stress-whitened region. The elastic stress distribution was used to analyse the very small zones observed in the initial non-linear region of the stress-displacement curve, zones such as those in Fig. 2. An approximate solution for the elastic stress distribution around a semicircular notch has been published [7] that is similar to the approximate solution frequently used to calculate stresses around a circular hole [8]. Although the solution for the hole gives the correct stress concentration factor and, therefore, is generally considered reliable, the semicircular notch calculation predicts a stress concentration factor of 2 rather than the correct value of 3, and was therefore considered to be inadequate for the purposes of this study which required the calculation of stresses very close to the notch surface. Several methods have been used to obtain the exact solution for the two-dimensional stress distribution around a semicircular edge notch in a semi-infinite plate under uniform tension [9–11]. These methods all give a maximum stress concentration factor of 3.065 at the notch root. The equations of Maunsell [9] were used because the series coefficients are available in the published literature.

After correction of typographical errors in the original published equation for the shear stress, the complete stress distribution of Maunsell is as follows

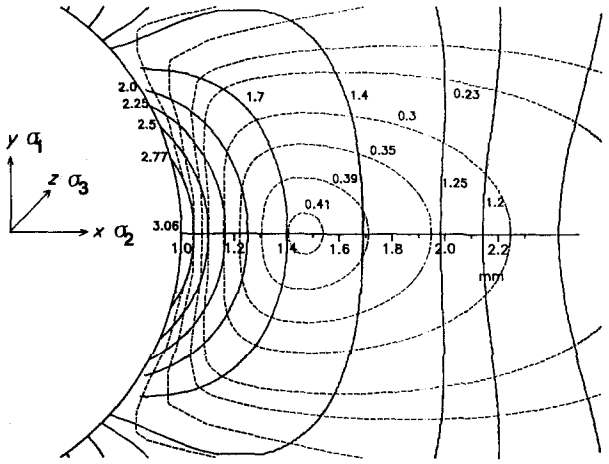

Figure 3 Major and minor principal stress contours at a semicircular notch with a radius of 1 mm. (——) σ_1 contours, and (– – –) σ_2 contours. Numbers indicate normalized stress values.

$$\sigma_{rr} = \sigma_0\left[\frac{1}{2}(1+\cos 2\theta) + \sum_{m=1}^{\infty}\frac{A'_m}{r^{2m+1}}\left(\sum_{n=0}^{\infty}(4n^2+2m-1)^m\alpha_n\cos 2n\theta\right) + \sum_{m=0}^{\infty}\frac{2(2m+1)B_m}{r^{2m+2}}[-m\cos 2m\theta + (m+2)\cos(2m+2)\theta]\right] \quad (1)$$

$$\sigma_{\theta\theta} = \sigma_0\left[\frac{1}{2}(1-\cos 2\theta) + \sum_{m=1}^{\infty}\frac{A'_m}{r^{2m+1}}\left(\sum_{n=0}^{\infty}2m(1-2m)^m\alpha_n\cos 2n\theta\right) + \sum_{m=0}^{\infty}\frac{2(2m+1)B_m}{r^{2m+2}}[m\cos 2m\theta - m\cos(2m+2)\theta]\right] \quad (2)$$

$$\sigma_{r\theta} = \sigma_0\left[-\frac{1}{2}\sin 2\theta + \sum_{m=0}^{\infty}\frac{A'_m}{r^{2m+1}}\left(\sum_{n=0}^{\infty}4nm^m\alpha_n\sin 2n\theta\right) + \sum_{m=0}^{\infty}\frac{2(2m+1)B_m}{r^{2m+2}}[-m\sin 2m\theta + (m+1)\sin(2m+2)\theta]\right] \quad (3)$$

where

$$^m\alpha_0 = \frac{16m^2-1}{2(4m^2-1)^2} \quad (4)$$

$$^m\alpha_n = \frac{16m^2-1}{[(2m+1)^2-4n^2][(2m-1)^2-4n^2]} \quad n>0 \quad (5)$$

where σ_0 is the remote stress, r and θ are the polar coordinates with the origin at the centre of the semicircle, A'_m and B_m are coefficients of the series satisfying the boundary conditions at the notch, and σ_{rr} and $\sigma_{\theta\theta}$ are the normal stresses and $\sigma_{r\theta}$ is the shear stress. The coefficients A'_m and B_m for the integer m ranging from 0 to 10 have been solved [9]. The infinite series solution is oscillatory with the index of truncation N and converges slowly to the true stress as the number of terms n increases. In this study, $n = N = 100$ was used and gave an error of 3%.

The solution for a semi-infinite plate has been modified for a strip of finite width by adding terms to account for edge effects [12]. The maximum stress concentration factor at the notch root is estimated to decrease from 3 to about 2.6 when the ratio of the width to notch radius is 20 to 1 [13]. Edge effects therefore introduce some uncertainty into the calculations, although the magnitude of the stresses may be affected more than the shape of the stress contours.

The major and minor in-plane principal stresses σ_1 and σ_2 were calculated from Equations 1, 2 and 3; a Quick BASIC program was developed to compute the

stress components in cartesian coordinates (x, y). These are plotted in Fig. 3 normalized to the remote stress, the contours differed significantly from those obtained with the approximate solution [7]. The σ_1 contours are curved near the notch tip as σ_1 decreases along the x-axis from a maximum normalized value of 3.065 at the root. The σ_2 contours change rapidly near the notch root increasing from zero at the notch surface to a maximum of 0.41 at a distance from the notch that is 0.47 times the notch radius. The minor principal stress is compressive in the region above and below the notch, the line of zero stress subtends an angle of 55° at the centre of the semicircle.

3.3. In-plane principal stresses at the damage zone boundary

The major and minor principal stresses along the boundary of the damage zone were obtained for several values of the remote stress σ_0. In order to assume that the presence of the damage zone did not disturb the elastic stress distribution, only photomicrographs of the small crescent-shaped damage zone obtained in the initial non-linear region of the stress–displacement curve were analysed. The boundary was determined from the projected image of the photographic negative which was enlarged 300 ×. The relationship between σ_1 and σ_2 is illustrated in Fig. 4 with data obtained at four remote stresses, the linear regression gave a slope of -0.69 with a correlation coefficient of -0.976. The major principal stress σ_1 at the boundary was greater than σ_2 and comparable in magnitude to the yield stress σ_y. Both σ_1 and σ_2 varied by about 10% along the boundary of the zone, σ_1 was highest at the notch surface and decreased towards the x-axis while σ_2 increased from the notch surface to the x-axis.

3.4. Through thickness stress

The damage zone was visible in the through thickness plane after the notch was removed by sectioning or polishing. The zone was very thin in the x direction so the 1.6 mm thick specimen shown in Fig. 5 was sectioned at a slight angle to the yz plane. A remnant of the notch is visible on the left-hand side and the damage zone is viewed at the notch surface. On the right-hand side of the micrograph, part of the damage zone was removed and the damage zone is seen some distance away from the notch surface along the x-axis. The damage zone was rectangular in shape and extended through the thickness except for a region at the edge with no stress-whitening that in width was 10 to 15% of the sheet thickness.

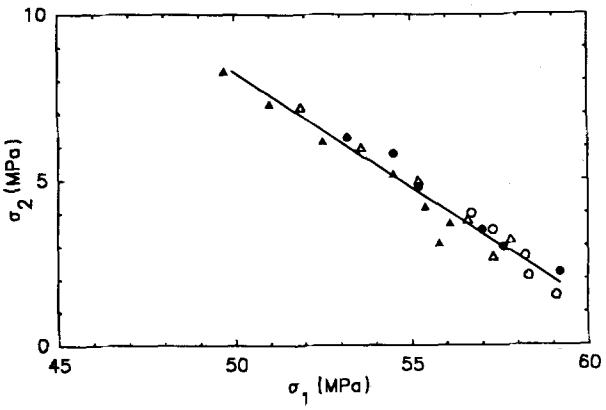

Figure 4 Values of σ_1 and σ_2 along the boundary of the stress-whitened zone of 3.6 mm thick PVC with 15 p.p.h. experimental resin 5896 at several remote stresses. (○ 21.6 MPa, ● 22.7 MPa, △ 23.2 MPa, ▲ 23.8 MPa).

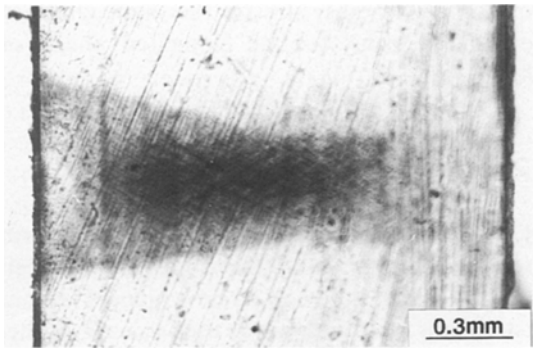

Figure 5 Optical micrograph of the stress-whitened zone of 1.6 mm thick PVC with 15 p.p.h. experimental resin 5896 loaded to 22.4 MPa and viewed in the yz plane after most of the notch was removed.

The through thickness stress is neither completely plane stress nor plane strain for a specimen with finite thickness. No solution for the three-dimensional elastic stress distribution in a notched thick plate is presently available. The closest case to a semicircular edge notch that has been treated is that of a circular hole in an infinite plate of finite thickness [14]. Here the approximate solution for the elastic stress distribution suggests that the plane strain condition is realized in the centre when the specimen thickness is at least four times the hole radius. Away from the notch root along the x-axis, the through thickness stress decreases rapidly. If the circular hole analysis were approximately valid for the semicircular notch geometry, it would predict a decrease in σ_3 of about 25% at a distance 0.2 mm from the notch root, approximately the length of the damage zone (cf. Fig. 2).

It is generally observed that the sharp notch geometry produces a state of plane strain through the thickness at the notch root except for a region near the surface where σ_3 decreases rapidly. Photoelastic methods have been used to determine experimentally the through thickness stresses in sharp notched specimens. For epoxy plates with notch depth to thickness ratio between 1 and 3, this boundary layer was observed to be 15% of the thickness [15]. In another study, this boundary layer was found to be only 5% of the thickness when the notch depth to thickness ratio was varied from 1.3 to 2.4, this result was consistent with three-dimensional finite element calculations [16]. Other finite element analyses have reported the boundary layer thickness variously from 7 to 10% of the thickness [17–22]. These observations apply to the through thickness stress at the notch root. The finite element analysis also predicts that σ_3 decreases rapidly away from the notch root in the x-direction. It is estimated that the distance away from the notch that

the plane strain condition holds is equal to about 5% of the thickness [21].

Comparison of the damage zone as it appeared in the *yz* plane with the results reported in the literature led to the conclusion that in the thickness direction the stress-whitened damage zone occurred in a region of plane strain. The region at the edge that was not stress-whitened was about 10 to 15% of the sheet thickness or roughly equal to the predicted width of the boundary layer of rapidly decreasing σ_3. The plane strain condition was also assumed in the *x*-direction where the crescent-shaped damage zone extended no more than 0.2 mm ahead of the notch root, or on the order of 6% of the thickness. The third principal stress σ_3 at the boundary of the damage zone was then calculated from the plane strain relationship $\sigma_3 = \upsilon(\sigma_1 + \sigma_2)$ using the Poisson's ratio of $\upsilon = 0.38$ reported for PVC [23].

3.4. Conditions for stress-whitening

The three principal stresses were always tensile stresses at the zone boundary, and typical values of σ_1, σ_2 and σ_3 when the remote stress was 22.7 MPa ranged from 59, 2.2 and 23 MPa, respectively, at the notch surface to 53, 6.3 and 23 MPa where the zone intersected the *x* axis. The slope of the linear relationship between σ_1 and σ_2 was close to unity, thus the value of σ_3 at the zone boundary was essentially constant. This suggested that a constant mean stress condition existed at the zone boundary, where the mean or hydrostatic stress is defined as $\sigma_m = (\sigma_1 + \sigma_2 + \sigma_3)/3$. Values of σ_m calculated around the boundary of the damage zone at four values of the remote stress were plotted in Fig. 6 for the blend with 15 p.p.h. of experimental resin 5896. The maximum variation in σ_m was about 5% from the average value of 28 MPa.

Comparison of the damage zone as it appeared at positions 1, 2 and 3 with the calculated mean stress contours for $\sigma_m = 28$ MPa (Fig. 7) showed how well the mean stress condition represented the shape of the damage zone. Some uncertainty in σ_m was due to the diffuseness of the boundary compared to the small size of the zone which measured no more than 0.2 mm along the *x*-axis. The small, gradual decrease in σ_m

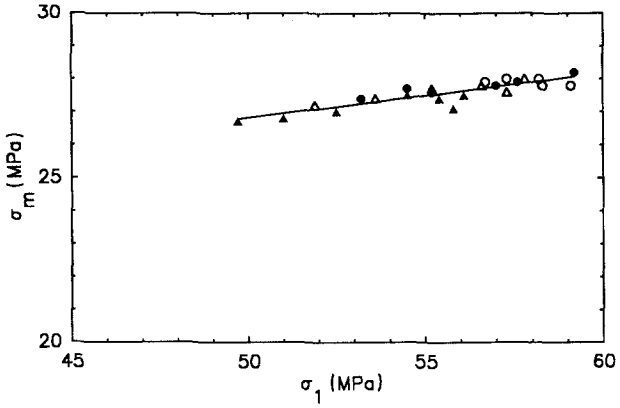

Figure 6 Mean stress along the boundary of the stress-whitened zone of 3.6 mm thick PVC with 15 p.p.h. experimental resin 5896 at several remote stresses. (○ 21.6 MPa, ● 22.7 MPa, △ 23.2 MPa, ▲ 23.8 MPa)

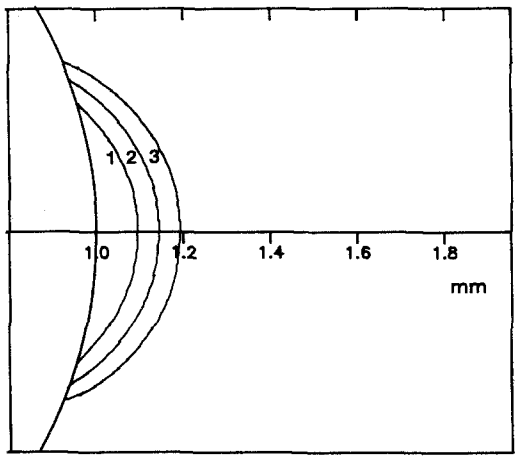

Figure 7 Calculated elastic mean stress contours at positions 1 (σ_0 = 21.6 MPa), 2 (σ_0 = 22.7 MPa) and 3 (σ_0 = 23.8 MPa) (cf. Fig. 2) for σ_m = 28 MPa.

around the boundary of the damage zone from the notch surface to the intersection with the *x*-axis could result from distortion of the elastic stress distribution by the presence of the damage zone.

The literature on ductile metals concerning cavity nucleation as a result of local plastic deformation indicates that there is a critical strain required for cavitation [24–26]. A strain criterion has also been suggested for crazing of polymers. Often a critical principal strain condition is considered [27, 28], but it has also been recognized that a dilational component must be involved and a critical volume strain for crazing of polycarbonate has been reported [29]. The critical elastic volume strain V_c was calculated from the mean stress and the bulk modulus

$$V_c = 3(1 - 2\upsilon)\sigma_m/E \quad (6)$$

where E is the measured Young's modulus. The value obtained, about 0.8%, was close to that reported for crazing in polycarbonate, 1.2% [29], and also close to that of ductile metals, about 1% [24].

Numerous microshear bands were observed when the damage zone was viewed in the *xy* plane (Fig. 8) or *yz* plane (cf. Fig. 5). Despite a superficial resemblance, these were not the α and β slip lines that emanate from the notch surface as the core yielding mode of polycarbonate [4] and PVC [30]. Differences were apparent in the shear angles, 53° to the *y*-axis for the microshear bands in the blend compared to 45° for core yielding, and also in the shape of the zone. The logarithmic trajectories of the α and β slip lines produce a characteristic shape of the core yielding zone [31] that does not resemble the shape of the stress-whitened zone. With the blends, it was inferred that cavitation, following the mean stress condition, was the initial microdeformation mechanism. Subsequently plastic deformation could occur more readily [32], and the localized shear yielding, visible as microshear bands, was nucleated by voids.

3.5. Compositional variables

Blends with 5, 10 and 20 p.p.h. of the experimental resin 5896 all exhibited a damage zone with the same

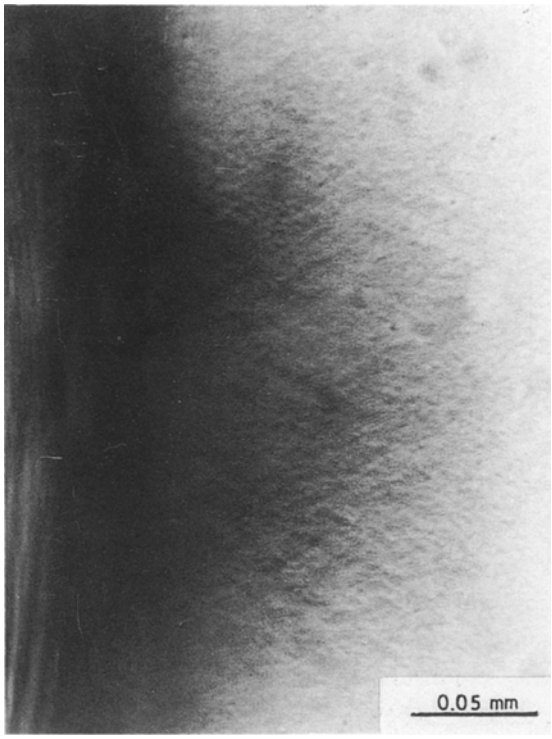

Figure 8 Optical micrograph of stress-whitened zone of 3.6 mm thick PVC with 15 p.p.h. experimental resin 5896 loaded at 28.2 MPa with the focus at the centre of the specimen.

TABLE I Mean stress and volume strain of PVC with experimental resin 5896

Experimental resin 5896 (p.p.h.)	Elastic Modulus[a] (GPa)	Yield Stress[a] (MPa)	σ_m		Volume Strain[a] (%)
			1.6 mm (MPa)	3.6 mm (MPa)	
5	3.2	57	34	33	0.7
10	2.6	51	29	29	0.8
15	2.5	49	26	28	0.8
20	2.3	44	20	23	0.7

[a] at 10 mm min^{-1} crosshead speed.

crescent shape described for the 15 p.p.h. blend. The critical mean stress calculated at the zone boundary for 3.6 mm thick sheet decreased from 33 MPa for 5 p.p.h. CPE to 23 MPa for 20 p.p.h. CPE, Table I. Results for the two thicknesses analysed, 3.6 and 1.6 mm, were the same within the experimental error of 10%. On the other hand, the critical volume strain, also included in Table I, was constant with an average value of 0.8%.

Blends were also prepared from a series of experimental CPE resins that differed in the percent chlorination and the amount of residual crystallinity as measured by heat of melting. These variables in the CPE affect a number of blend properties including the ductile-to-brittle transition and transparency [5]. Those blends that were sufficiently transparent at the 5 and 20 p.p.h. level for the damage zone to be visible in the optical microscope were analysed in the same manner as the blends with experimental resin 5896. The value of σ_m determined on 1.6 mm thick sheet was the same for all the experimental resins examined. For 5 p.p.h. this value was 33 ± 1 MPa and for 20 p.p.h. was 23 ± 1 MPa (Table II).

Although the critical volume strain concept gave a consistent description of the stress-whitened zone, it is generally recognized that at the microscopic level of the CPE particles, the heterogeneous blend morphology creates a microstress state that is significantly different from the macroscopic stress state. In particular, interaction of the stress fields around individual particles can increase the local stress concentration factor and this has been cited as a factor leading to enhanced matrix ductility [33, 34]. The possibility that overlap of local stress fields might have affected the conditions for formation of the stress-whitened zone, particularly when the amount of CPE was increased, was therefore examined. Experimental evidence has been presented to suggest that overlap only becomes significant when the particle separation is equal to the particle radius [35], or when the volume fraction is about 0.2. Analytically, the exact solution for the elastic stress distribution between two circular holes [36], with the centre-to-centre distance calculated for a close-packed arrangement of 0.5 μm particles, and the approximate solution for finite concentration of spherical voids [37] gave the same results. The predicted elastic stress concentration factor increased only slightly over the composition range employed, increasing from 2.4 for 5 p.p.h. CPE to 2.8 for 20 p.p.h. compared to about 2 for an isolated sphere. It was, therefore, concluded that changes in the local stress concentration factor due to overlapping stress fields were negligible in this case.

3.6. Temperature variable

An analysis was made of the damage zone that formed when the blend with 10 p.p.h. of the experimental resin 5896 was deformed at several temperatures between ambient and $-40\,^{\circ}C$. In all cases, the initial deformation observed in the 1.6 mm thick specimens was the formation of a crescent-shaped stress-whitened zone ahead of the semicircular notch. At higher stresses the zone became elongated ahead of the notch. Fracture subsequently occurred by ductile tearing at the higher temperatures, or sometimes by rapid propagation of a brittle crack through the damage zone at the lowest

TABLE II Mean stress of 1.6 mm thick PVC with 5 and 20 p.p.h. experimental CPE resins

Experimental CPE	Cl (%)	T_g (1 Hz) (°C)	ΔH_m $(J\,g)^{-1}$	σ_m	
				5 p.p.h. (MPa)	20 p.p.h. (MPa)
5879	28.9	−19	0.4	33.3	–
5881	29.3	−18	9.2	33.9	22.8
5890	34.7	−19	0.4	34.2	–
5908	34.1	−12	8.0	31.5	22.6
5892	39.3	−14	0.4	33.2	22.4
5894	39.4	−2	10.5	33.4	23.7
5888	44.6	10	2.9	35.2	22.6
5896	45.6	17	10.0	33.8	20.0

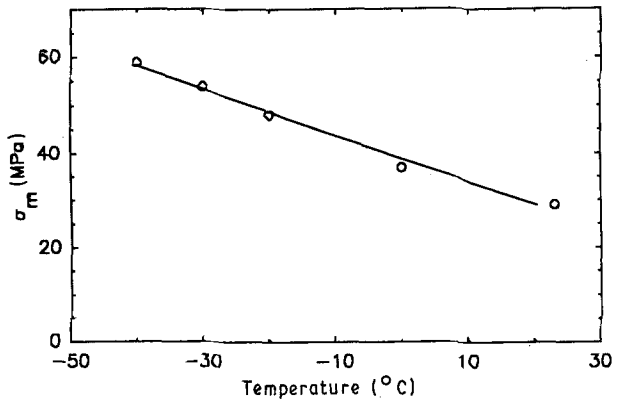

Figure 9 Mean stress along the boundary of the stress-whitened zone of 1.6 mm thick PVC with 10 p.p.h. experimental resin 5896 as a function of temperature.

TABLE III Mean stress and volume strain of 1.6 mm thick PVC with 10 p.p.h. experimental resin 5896 at different temperatures

Temperature (°C)	Modulus (GPa)	Mean stress (MPa)	Volume strain (%)
23	2.6	29	0.7
0	3.5	37	0.8
− 20	3.7	48	0.9
− 30	4.7	54	0.8
− 40	4.9	59	0.9

temperatures, − 30 and − 40 °C. The critical mean stress calculated at the zone boundary increased in a linear manner with decreasing temperature from 29 MPa at ambient temperature to 59 MPa at − 40 °C (Fig. 9). The linear relationship between temperature T and σ_m was given by $\sigma_m = -0.49T + 39$ ($r = -0.995$), and extrapolated to $T = 80$ °C, approximately the glass transition temperature, when $\sigma_m = 0$.

The critical elastic volume strain V_c was calculated according to Equation 6 using the bulk modulus obtained from the temperature dependent Young's modulus, and was found to be constant with a value of about 0.8%, Table III. This led to the conclusion that the parameter controlling cavitation was the critical volume strain. Furthermore, it appeared that the critical volume strain was a material property of PVC since it did not depend on the amount of the second phase nor did it depend on whether the second phase was in the rubbery state, as were most of the CPE resins at ambient temperature, or in the glassy state, as in the low temperature determinations.

3.7. Plastic zone

To discuss the shape of the zone at higher stresses, it was necessary to assume that the stress-whitened damage zone was a plastic zone in an otherwise elastic material. The assumption that the elastic stress distribution could be used to obtain the elastic–plastic boundary was only successful when the damage zone was small. At higher stresses, the effects of stress redistribution caused by the presence of the plastic zone, and by distortion of the notch shape from semicircular, were not negligible. As a result, the crescent shape was lost, and the zone became elongated ahead of the notch as shown at position 4 on the stress–displacement curve (27.0 MPa, Fig. 10a) and at position 5 (31.5 MPa, Fig. 10b).

Evolution of the zone shape was consistent with concepts from the literature that describe the stress redistribution when a plastic zone is present ahead of the notch. Finite element analysis in the case of plane strain bending has shown that the position of maximum σ_1 is near the elastic–plastic boundary and moves away from the root of the Charpy notch as the remote stress increases [38]. Movement of the position of maximum σ_1 away from the notch root in a direction perpendicular to the remote stress has been confirmed with other notched geometries [39, 40]. The shape of the elastic–plastic boundary produced by

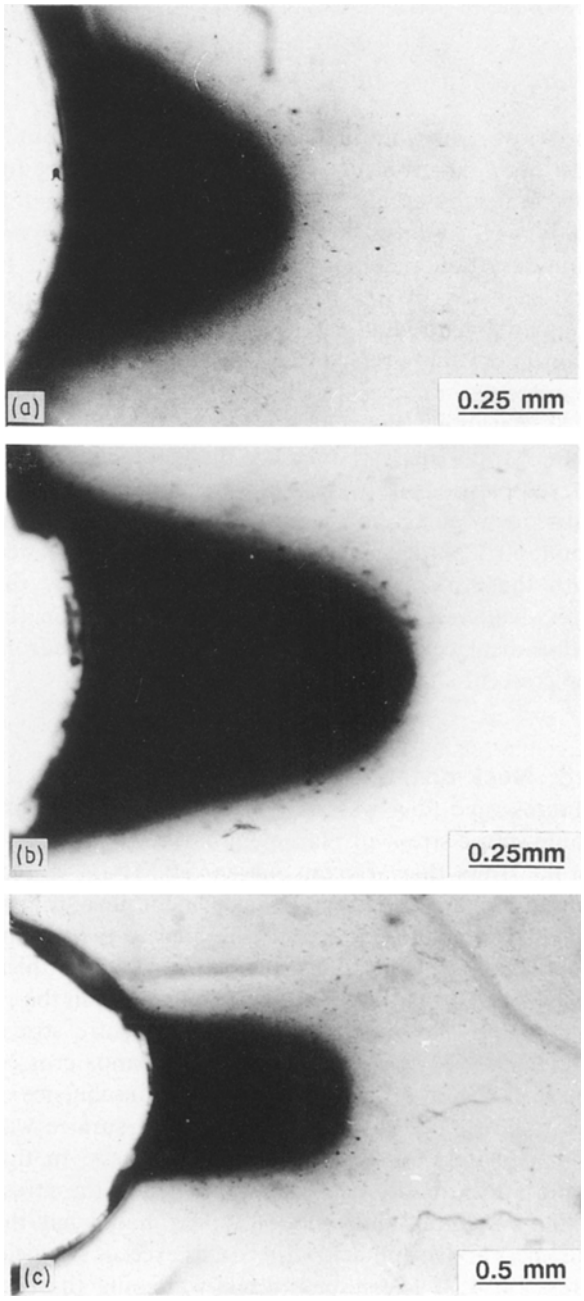

Figure 10 Optical micrographs of stress-whitened zone of 3.6 mm thick PVC with 15 p.p.h. experimental resin 5896. (a) Position 4, 27.0 MPa, (b) position 5, 31.5 MPa, and (c) position 6, 35.0 MPa.

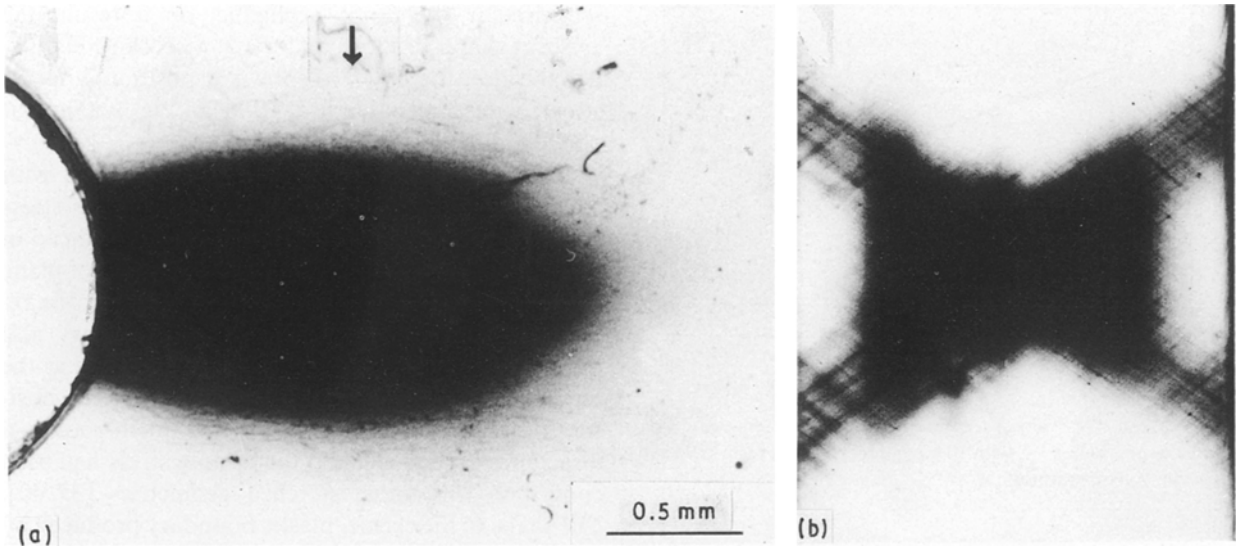

Figure 11 Optical micrographs of (a) stress-whitened zone of 1.6 mm thick PVC with 5 p.p.h. experimental resin 5896 at 40.0 MPa, and (b) stress-whitened zone sectioned at the position of the arrow in (a) and viewed in the *yz* plane from the notch side.

the stress redistribution ahead of a semicircular notch has been determined by photoelastic methods for sheet thicknesses comparable to those used in this study [41–43]. In these cases, the initial curved boundary became elongated with a shape similar to that depicted in Fig. 10. The zone shape was also compared with that deduced for the elastic–plastic solution of the stress distribution obtained for two semicircular notches by a finite difference method [44]. Assuming the von Mises yield condition, the plane strain analysis predicts the appearance of a curved plastic zone at 33% of the yield stress and the subsequent elongation along the *x*-axis beginning at about 50% of the yield stress. These closely correlated with the remote stresses at which respectively the stress-whitened zone appeared at position 1 on the stress–displacement curve, and began to deviate from the crescent shape at position 4.

3.8. Neck instability

Macroscopic flow was only detected near the maximum in the stress–displacement curve. At position 6 on the stress–displacement curve (35.0 MPa, Fig. 10c) thinning of a necked region was evident ahead of the notch. The macroscopic flow that created the dimensional change was apparent when a 1.6 mm thick specimen (Fig. 11a) was polished and viewed in the *yz* plane, Fig. 11b. Superimposed on the centre stress-whitened zone, two intersecting shear bands crossed the thickness at an angle of 53°. As a consequence of the shear angle, the zone width on the surface was approximately equal to the plate thickness. In this plane stress mode, necking occurs when the stress acting on regions a distance of approximately half the thickness above and below the *x*-axis exceeds the yield stress [4, 45]. The intense stress-whitening that accompanied the intersecting shear mode was caused by triaxiality developed in the neck [46, 47].

The macroscopic plane strain shear mode observed in materials such as polycarbonate [4] and silicon steel [45] is through thickness yielding or hinge shear on inclined planes above and below the notch root. A side view of a thicker (3.6 mm) blend specimen did not show hinge shear yielding, Fig. 12a, instead the necked zone was similar in appearance to that of the thinner specimen. A view of the thicker specimen in the *yz* plane, Fig. 12b, showed that instead of shear on through thickness planes, the stress-whitened zone relieved constraints in the thickness direction. Near each edge where σ_3 decreased rapidly and the stress-whitening condition was not achieved, two macro-shear bands extended above and below the stress whitened zone at an angle of about 53°. Thinning between the two shear bands confirmed the plane stress condition of this region. A similar zone has been observed in sheets comprised of many alternating layers of PC and SAN; in this case crazing of the SAN layers relieved the triaxiality in the centre region. During fracture, extension of the material in the plane stress region near the edges can create the shear lips that characterize fracture surfaces of microlayer sheets [48] and PC/ABS blends [49].

The toughening of thick sheet that occurs when a second phase promotes cavitation can be seen in several stages. As the initial irreversible deformation event, cavitation relieves triaxiality and in addition absorbs energy by localized flow of the matrix. The large amount of ductile deformation that accompanies cavitation is apparent when fracture surfaces of the stress-whitened region are viewed in the SEM. Strain hardening of the deformed matrix stabilizes the voids and unlike ductile metals, cavitation is not immediately followed by coalescence and fracture; instead, when the instability conditions are achieved macro-shear bands form in the plane stress region near the edge. With the triaxiality removed, energy can be absorbed before and during fracture by ductile flow in the plane stress region to create the shear lips that characterize fracture surfaces of many polymer blends.

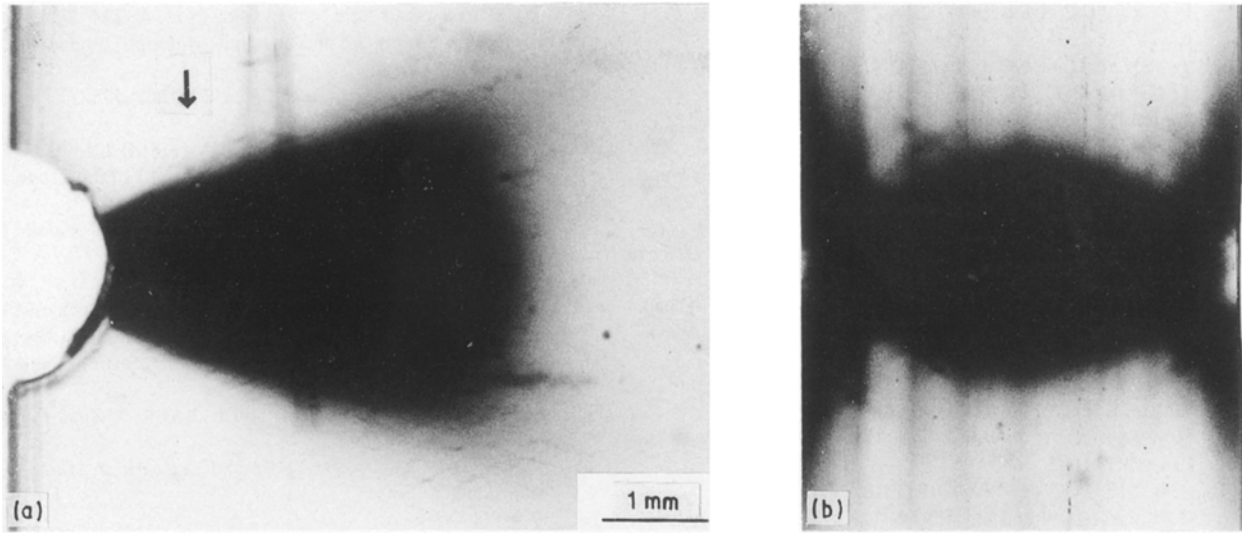

Figure 12 Optical micrographs of (a) stress-whitened zone of 3.6 mm thick PVC with 5 p.p.h. experimental resin 5896 at 45.0 MPa, and (b) stress-whitened zone sectioned at the position of the arrow in (a) and viewed in the *yz* plane from the notch side.

4. Conclusions

The use of experimental CPE resins that formed translucent blends with PVC made it possible to view the stress-whitened zone in thick sheets by conventional optical microscopy. Analysis of the zone that formed ahead of a semicircular notch during slow tensile loading led to the following conclusions.

1. The shape of the initial small crescent-shaped zone was described by a mean stress condition using the plane strain elastic stress distribution. The bulk modulus was used to calculate a critical volume strain for stress-whitening. This quantity was independent of composition and temperature, and was thought to be the controlling parameter for cavitation.

2. The observation that the material followed a mean stress condition suggested that cavitation was the initial microdeformation mechanism. The profuse microshear banding visible in the damage zone was thought to nucleate subsequently from the voids.

3. Concepts of stress redistribution that determine the elastic–plastic boundary qualitatively described the shape of the zone at higher loading.

4. Macroscopic flow was only detected near the maximum in the stress–displacement curve. In thinner sheet, the plane stress intersecting shear mode produced a necked region; while in thicker sheet, the cavitation zone relieved the through thickness constraint and necking was produced by macroshear bands in the plane stress region near the edge.

Acknowledgements

This research was generously supported by The Dow Chemical Company, Louisiana Division, Plaquemine, LA, and the National Science Foundation, Polymers Program (DMR 87-13041).

References

1. A. SIEGMANN and A. HILTNER, *Polym. Eng. Sci.* **24** (1984) 869.
2. A. SIEGMANN, L. K. ENGLISH, E. BAER and A. HILTNER, *ibid.* **24** (1984) 877.
3. A. G. EVANS, Z. B. AHMAD, D. G. GILBERT and P. W. R. BEAUMONT, *Acta Metall.* **34** (1986) 79.
4. M. MA, K. VIJAYAN, J. IM, A. HILTNER and E. BAER, *J. Mater. Sci.* **24** (1989) 2687.
5. A. TSE, R. LAAKSO, A. HILTNER and E. BAER, *J. Appl. Polym. Sci.* in press.
6. J. F. KNOTT and A. H. COTTRELL, *J. Iron Steel Inst.* **201** (1963) 249.
7. E. G. COKER and L. N. G. FILON, "Photoelasticity" (Cambridge University Press, Cambridge, 1931) p. 163.
8. S. TIMOSHENKO and J. N. GOODIER, "Theory of Elasticity" 3rd Edn (McGraw-Hill, New York, 1961) p. 90.
9. F. G. MAUNSELL, *Phil. Mag.* **21** (1936) 765.
10. C. B. LING, *J. Math. Phys.* **26** (1947) 284.
11. O. L. BOWIE, *ibid.* **45** (1966) 356.
12. C. B. LING, "Mechanics of Fracture 5: Stress Analysis of Notch Problems" edited by G. C. Sih (Martinus Nijhoff, The Hague, 1978) p. 135.
13. N. NODA and H. NISITANI, *Engng Fract. Mech.* **28** (1987) 223.
14. E. STERNBERG and M. A. SADOWSKY, *J. Appl. Mech.* **16** (1949) 27.
15. J. R. DIXON, in "Physical Basis of Yield and Fracture: Conference Proceedings" Vol. 1 (Institute of Physics & The Physical Society, London, 1967) p. 6.
16. G. VILLARREAL and G. C. SIH, "Mechanics of Fracture 7" edited by G. C. Sih (Martinus Nijhoff, The Hague, 1981) p. 253.
17. N. LEVY, P. V. MARCAL and J. R. RICE, *Nucl. Engng Design* **17** (1971) 64.
18. D. M. TRACEY, *ibid.* **26** (1974) 282.
19. P. D. HILTON, "Mechanics of Fracture 3" edited by G. C. Sih (Noordhoff, Leyden, 1977) p. 273.
20. A. J. ROSAKIS and K. RAVI-CHANDAR, *Int. J. Solids Struct.* **22** (1986) 121.
21. T. NAKAMURA and D. M. PARKS, *J. Appl. Mech.* **55** (1988) 805.
22. I. D. PARSONS and J. F. HALL, *Engng Fract. Mech.* **33** (1989) 45.
23. E. A. COLLINS, C. A. DANIELS and C. E. WILKES, "Manual of Physical Constants of PVC" (The BFGoodrich Co., Avon Lake, OH, 1974) p. 47.
24. S. H. GOODS and L. M. BROWN, *Acta Metall.* **27** (1979) 1.
25. R. D. THOMSON and J. W. HANCOCK, *Int. J. Fract.* **26** (1984) 99.
26. J. T. BARNBY, C. J. FLAVELL, A. S. NADKARNI and Y. W. SHI, "Proceedings of the 4th International Conference on Fracture" edited by S. R. Valluri, D. M. R. Taplin,

P. R. Rao, J. F. Knott and R. Dubey (Pergamon, Oxford, 1984) p. 1287.
27. T. T. WANG, M. MATSUO and T. K. KWEI, *J. Appl. Phys.* **42** (1971) 4188.
28. J. MILTZ, A. T. DIBENEDETTO and S. PETRIE, *J. Mater. Sci.* **13** (1978) 1427.
29. R. P. KAMBOUR, M. A. VALLANCE, E. A. FARRAYE and L. A. GRIMALDI, *ibid.* **21** (1986) 2435.
30. A. TSE, E. SHIN, A. HILTNER and E. BAER, *ibid.* in press.
31. R. HILL, "The Mathematical Theory of Plasticity" (Oxford University Press, Oxford, 1950) p. 250.
32. A. J. KINLOCH, "Rubber-Toughened Plastics" (Adv. Chem. **222**) edited by C. K. Riew (American Chemical Society, Washington, 1989) p. 67.
33. S. WU, *Polymer* **26** (1985) 1855.
34. S. WU, *J. Appl. Polym. Sci.* **35** (1988) 549.
35. M. MATSUO, T. T. WANG and T. K. KWEI, *J. Polym. Sci.* **10A** (1972) 1085.
36. C. B. LING, *J. Appl. Phys.* **19** (1948) 77.
37. G. P. TANDON and G. J. WENG, *J. Appl. Mech.* **53** (1986) 511.
38. J. R. GRIFFITHS and D. R. J. OWEN, *J. Mech. Phys. Solids* **19** (1971) 419.
39. R. TWICKLER, M. TWICKLER and W. DAHL, *Engng Fract. Mech.* **24** (1986) 553.
40. D. M. TRACEY and C. E. FREESE, ASTM STP 995, (American Society for Testing and Materials, Philadelphia, 1989) p. 93.
41. P. S. THEOCARIS, *J. Appl. Mech.* **29** (1962) 735.
42. *Idem., Exp. Mech.* **3** (1963) 207.
43. G. U. OPPEL and P. W. HILL, *ibid.* **4** (1964) 206.
44. D. N. DE G. ALLEN and R. SOUTHWELL, *Phil. Trans. R. Soc.* **242** (1950) 379.
45. G. T. HAHN and A. R. ROSENFIELD, *Acta Metall.* **13** (1965) 293.
46. P. W. BRIDGMAN, *Trans. ASM* **32** (1944) 553.
47. T. SUZUKI and S. YANAGIMOTO, "Fracture Mechanics of Ductile and Tough Materials and its Applications to Energy Related Structures" edited by H. W. Liu (Martinus Nijhoff, The Hague, 1981) p. 179.
48. M. MA, J. IM, A. HILTNER and E. BAER, *J. Appl. Polym. Sci.* **40** (1990) 669.
49. M. LEE, C. KAO, A. HILTNER and E. BAER, *J. Mater. Sci.* submitted.

Received 11 June
and accepted 1 August 1990